Bull. Chem. Soc. Ethiop. **2025**, 39(2), 271-286.
DOI: https://dx.doi.org/10.4314/bcse.v39i2.7

ISSN 1011-3924
Printed in Ethiopia
Online ISSN 1726-801X

GREEN SYNTHESIS, CHARACTERIZATION, ANTIMICROBIAL AND ANTI-CANCER ACTIVITY OF SILVER NANOPARTICLES USING *ARISTOLOCHIA BRACTEOLATE* PLANT LEAF EXTRACT: EXPERIMENTAL AND THEORETICAL CALCULATIONS

P. Durairaju[1], G. Raja[2], G. Venkatesh[3*], C. Govindasamy[4], Ahmed S. El Newehy[4], S. Haseena[5], P. Vennila[6] and S. Balasubramaniyan[7]

[1,6]Department of Chemistry, Thiruvalluvar Government Arts College, Rasipuram–637 401, India
[2]Department of Chemistry, Paavai Engineering College (Autonomous), Namakkal, Tamil Nadu 637018, India
[3]Department of Chemistry, Muthayammal Memorial College of Arts & Science, Namakkal-637408, India
[4]Department of Community Health Sciences, College of Applied Medical Sciences, King Saud University, Riyadh 11433, Saudi Arabia
[5]Department of Physics, Muthayammal Memorial College of Arts & Science, Namakkal-637408, India
[7]Department of Pharmaceutical Technology, Anna University, BIT Campus, Trichy, 620024, India

(Received August 4, 2024; Revised October 3, 2024; Accepted October 4, 2024)

ABSTRACT. Silver nanoparticles were synthesized using *Aristolochia bracteolate* plant extracts. The nanoparticles were subsequently studied using various techniques such as UV-Vis, FTIR, EDS, XRD, SEM, and HR-TEM analysis. MTT assays have been utilized to determine the cytotoxicity of green synthesized silver nanoparticles at concentrations ranging from 2.5 to 15 µg. The Ab-AgNPs exhibited effective cytotoxic activity against MCF-7. Anticancer activity studies revealed that Ab-AgNps produced comparable good results for standard cancer drugs. Ab-AgNPs are used for evaluating their antibacterial effectiveness against pathogenic gram-positive and gram-negative bacteria. Aristolochic acid (AA1) and Aristolochic acid (AA2) are the major phytoconstituents in the *Aristolochia bracteolate*. The current study reports theoretical investigations of aristolochic acids (AA1 and AA2) as well as silver nanocages aristolochic acids using density functional theory. Furthermore, the silver-doped with Aristolochic acids (AA1 and AA2) was subjected and examined their of breast cancer activity using molecular docking analysis.

KEY WORDS: Aristolochia bracteolate, Silver nanoparticles, Transmission electron microscopy, Docking, Anti cancer active

INTRODUCTION

Breast cancer is the most prevalent malignancy among women and ranks second in terms of cancer-related mortality. It is the fifth most prevalent cancer associated with mortality on a global scale [1-5]. It is exceedingly challenging to decipher the molecular puzzle of the disease due to the intricate cellular mechanisms of cancer cells. Breast cancer is a chronic condition that is hypothesized to be an assemblage of discrete diseases that primarily induce genetic alterations in cells. Breast cancer research can benefit from MCF-7 cells due to their numerous distinctive characteristics that are also present in the mammary epithelium. It pertains to the capacity of MCF-7 cells to metabolize estradiol, an estrogen derivative, through estrogen receptors located in their cytoplasm [6-9].

*Corresponding authors. E-mail: venkateshindhuja@gmail.com

Nanotechnology has also paved the way for significant advancements in the field of medicine. The use of nanomaterials for targeted drug delivery has shown great promise in minimizing drug degradation and side effects, while increasing bioavailability [1]. Additionally, the utilization of plant products for nanoparticle synthesis has opened up new possibilities in the field of nano biotechnology. Through the utilization of natural sources like plants, bacteria, fungi, and algae, the production of metal oxide particles can be achieved on a large scale, ensuring purity and minimizing impurities. These advancements in nanoparticle synthesis have broadened the possibilities for obtaining particles with specific characteristics, further expanding the potential applications of nanotechnology in medicine and molecular biology [3-6]. The field of study on green-synthesized AgNPs is rapidly growing due to their significant potential activity. Phytoconstituents from plants, used for green synthesis, provide a wide range of potent medications with exceptional efficacy in combating severe diseases like cancer and viral infections. The dimensions, morphology, and electrostatic potential of AgNPs directly influence their biological reactivity. Therefore, a comprehensive analysis of pharmacodynamics and pharmacokinetics is necessary in order to comprehend the precise mechanism, distribution, toxicity, and adverse effects [7-10].

Synthesis of metal nanoparticles for biocompatible nanomedicine development is one of the most promising goals of modern research. The remarkable physical, chemical, and antibacterial characteristics of silver nanoparticles have prompted a great deal of study [8-10]. The biotherapeutic activities of leaf extracts of *Aristolochia bracteolata* were investigated; among an assortment of aqueous and chloroform solvents, the methanolic extract exhibited the greatest activity. *Aristolochia bracteolata* methanolic extracts were tested against moraxella catarrhalis, and the results show that aristolochic acid is essential antibacterial activity [8]. Amit et.al, studied the effectiveness of *Aristolochia bracteolata* lam aqueous extract on a worm-infested wound [9]. *Aristolochia bracteolata* shoot AgNPs exhibit excellent antioxidant activity [10]. The study discovered that A. bracteolate aqueous leaf extract is capable of manufacturing AgNPs, which have the capability to successfully kill C. quinquefasciatus juveniles with only a small quantity. A phytofabrication of AgNPs has been accomplished using an aqueous extract of *Aristolochia bracteolata*, and the investigation's conclusions showed antioxidant capacity, antibacterial activity against pathogenic organisms, and malarial insecticide properties [11]. According to an examination of literature, *Aristolochia bracteolate* plants serve as a medicinal plant [8-12]. The cytotoxicity of AgNPs toward human cancer cell lines, as well as their antileishmanial and antibacterial properties, was examined using *Scrophularia striata* extract [5]. The antitumor effect of silver nanoparticles in Tamarindus indica is investigated using the MCF-7 human breast cancer cell line [6]. Nanocages have been studied for their potential role in delivering a range of anti-cancer drugs inside the body using the nanoscale drug carrier technique. An additional possible property of metal-based nanocages is their detectable surface plasmon resonance effect, particularly those composed of iron, gold, and silver [13]. Computational methods can enhance comprehension of molecular structures and predict the physical and chemical properties of compounds. Density functional theory (DFT) is a widely used quantum-mechanical method in materials modeling. Several published studies have provided evidence of its effectiveness in investigating the local reactivity properties of molecules and assessing the binding strengths between molecular structures [14-19].

In this study, silver nonoparticles have been synthesized using *Aristolochia bracteolata* leaves and flowers extracts. Structural characterization of synthesized *Aristolochia bracteolata* nanoparticles (Ab-AgNPs) has been carried out using UV-Vis, XRD, SEM, HR-TEM, and FTIR spectroscopy. In addition, the biological activity of silver nanoparticles has been evaluated against both gram-positive and gram-negative microorganisms. Previous studies [20, 21] have documented that Aristolochic acids ((AA1(8-methoxy-6-nitrophenanthro[3,4-d][1,3]dioxole-5-carboxylic acid) and AA2 (8-methoxy-6-nitrophenanthro[3,4-d][1,3]dioxole-5-carboxylic acid)) are predominantly present in the plants of *Aristolochia bracteolata*. Aristolochic acids (refer

Scheme 1) were optimized using the B3LYP functional 6-311++G (d,p) basic set and nanocaged with silver atoms; their physicochemical properties were investigated. Furthermore, silver doped with aristolochic acids (AA1 and AA2) was tested for breast cancer activity using molecular docking analysis.

EXPERIMENTAL

Preparation of plant extract

The leaves of *Aristolochia bracteolate* had been obtained from the botanical garden situated on our college campus. The specimen was subsequently taxonomically recognised and authenticated by the Department of Botany. Four to five times, the leaves were rinsed with tap water prior to drying at room temperature in the shade. The desiccated leaves were subsequently blended with an electric laboratory blender to a fine powder. In order to create the extract, 200 mL of deionized water was mixed with 20 g of finely ground *Aristolochia bracteolate* plant powder. The mixture was then heated to a temperature of 100°C and maintained at that temperature for a period of 20 to 30 min. The extracted solution was filtered using filter paper (Whatman no.1) and stored at 4 °C for future use. The extract was kept at 4 °C until it was needed.

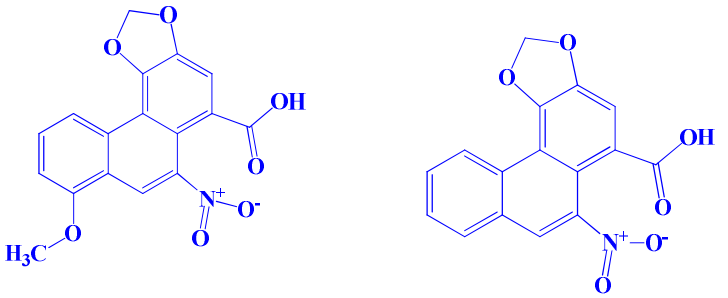

8-methoxy-6-nitrophenanthro[3,4-d][1,3]dioxole-5-carboxylic acid (AA1)

6-nitrophenanthro[3,4-d][1,3]dioxole-5-carboxylic acid (AA2)

Scheme 1. Important macromolecules of *Aristolochia bracteolate.*

Preparation of silver nanoparticles

A freshly prepared 100 mL of 0.1 mM $AgNO_3$ solution was mixed with 20 mL of *Aristolochia bracteolate* leaf extract and incubated in a shaker incubator at 300 rpm for 48 hours at 37 °C. It has been observed that the solution undergoes a reddish brown-brown color change, suggesting the formation of AgNPs (Figure 1). This indicates that the aqueous extract of plant parts may have successfully reduced aqueous silver ions, resulting in the production of highly stable silver nanoparticles. Leaf extract of *Aristolochia bracteolate* was utilized to examine the reduction of silver nitrate.

Characterization of AB-AGNPS

The UV-Vis spectra were acquired utilizing a UV-Vis Perkin Elmer Lambda 365 spectrophotometer, which possessed a range of 220–600 and a resolution of 1 nm. Plant extract and Ab-AgNPs functional groups were analyzed using the KBr pellet approach on FTIR spectrophotometer. The FTIR had a scanning range of 4000–400 cm^{-1} and a wavelength resolution of 1 cm^{-1}. The XRD technique was employed to ascertain the particle size and composition of the silver nanoparticle using a Shimadzu XRD-6000/6100 model with 30 kV, 30 mA, and Cu kα radians at a 2θ angle, this was performed. The size, shape, and morphology of the particles were

investigated using high resolution electron microscopy at 200 kV and transmission electron microscopy (TEM).

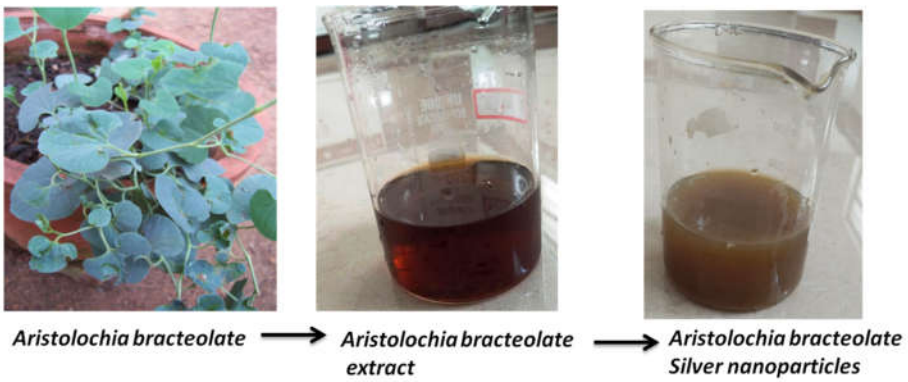

Figure 1. Synthetic routs for *EA-AuNPS.*

MTT assay

A method developed by Mosmann *et al.* was [22] employed to assess the cytotoxic effects of Ab-AgNPs on MCF-7 human breast cancer cells. A comprehensive procedure can be obtained in the supplementary file.

Antioxidant activity analysis

The DPPH method [23, 24] was used to determine Ab-AgNPs' free radical scavenging activity; a detailed procedure is provided in the supplementary file.

Computational study

Quantum chemical calculations were performed using Gaussian 16 software [25], employing the B3LYP functional and 6-311++G(d,p) basis set. The quantum descriptor isosurface mapping was generated using the Gauss View 6.0 [26] molecular editor and visualization software, utilizing the output files produced by Gaussian. This energy level and method is more reliable for analysis of molecular structural behaviour and their thermodynamic parameters and also it utilized in further studies. In this study, macromolecules (AA1 and AA2) and nano cages (AA1-Ag6 and AA2-Ag6) were optimized and their physicochemical properties were investigated. The Frontier molecular orbital (HOMO and LUMO) calculations were performed at the same level of theory, and the results were used to determine their global reactivity parameters, which included ionization potential, hardness, softness, and electronegativity [27-31]. Chemical potential parameters were also assessed using Koopman's theorem [27], as described by Parr and Pearson [28, 29]. Furthermore, the molecular electrostatic potential (MEP) images also created with help of same level theory, the images were utilized to determine the interaction of electron within the whole system.

RESULTS AND DISCUSSION

Phytochemical analysis

Qualitative screening of phytochemicals was conducted on leaf extracts of *Aristolochia bracteolate* [32]. The qualitative analysis of the aqueous leaf extract of *Aristolochia bracteolate*

identifies the several phytochemical elements that are responsible for reducing and capping AgNps. The phytochemical screening of the aqueous leaf extract of *Aristolochia bracteolate* revealed that it contains a significant amount of secondary metabolites. A study has been conducted on the chemical composition of the leaf extracts of *Aristolochia bracteolata* using water solvent. The analysis revealed the presence of phytochemicals that are similar to those found in previous studies. These phytochemicals likely cause the decrease in silver and function as a capping agent to avoid the clumping together and maintain the stability of the nanoparticles. Polar solvents are most effective for extracting polar phytochemicals, which are crucial for nanoparticle synthesis.

UV-Vis spectral analysis

The formation of AgNPs can be detected using UV-Visible spectroscopy, which is a basic but highly sensitive methodology. Ab-AgNPs had a broad absorption band centered at 425.88 nm, whereas *Aristolochia bracteolate* extracts did not show any discernible absorption peak in the 400-800 nm wavelength regions [33-35]. The observed strong broad absorption peak of silver nanoparticles suggests that the spherical particles existed without aggregation. Detailed surface plasmon resonance (SPR) is the term used to describe this absorption band. The SPR peak for spherical silver nanoparticles synthesized was also reported in the same region. The reduction of silver ions (Ag^{+}) to metallic silver nanoparticles (Ag^{0}) in the current system is thus revealed by the observed SPR peak in Ab-AgNPs.

FTIR vibrational spectra analysis

FTIR spectroscopy was used to recognize the chemical components of the samples. The vibrational spectra of *Aristolochia bracteolata* extract and Ab-AgNps correspond to the distinct functional groups. In general, the O–H bond of stretching vibration manifests itself between 3600 and 3400 cm^{-1} [36, 37]. Phenolic groups are present in the extract of *Aristolochia bracteolata*; the OH stretching band arises at 3426 cm^{-1}. The analysis of *Aristolochia bracteolate* plant extracts may also yield evidence for the existence of phenolic compounds. The CH_3 asymmetric and symmetric modes were identified at 2926 and 2824 cm^{-1}, correspondingly [38]. Two prominent peaks at 1634 and 1384 cm^{-1} indicate symmetric and anti-symmetric C=O stretching vibrations of carboxylic acid groups, accordingly. The C-C and C-N vibrational spectra were found at 1455 and 1040 cm^{-1}, respectively. Peaks 1285 and 761 cm^{-1} indicate the presence of in-plane and out-of-plane bending C-H bonds. FTIR spectra confirmed the existence of the stabilising compounds on the surface of the silver nanoparticles that were synthesised. *Aristolochia bracteolata* extract after Ab-AgNPs, the phonolic group vibration spectra were also found at 3426.41 cm^{-1}, suggesting that it may develop biological activities. The conjugation of carboxyl C=O bond mode was also discovered at 1635 and 1385 cm^{-1}. The peak at 662 cm^{-1} represents the Ago stretching band of magnetite. The occurrence of functional groups could be attributed to the incorporation of plant extracts, whilst the hydroxyl interaction can be assigned to the metal surface's absorption of water component.

Scanning electron microscopy (SEM) analysis

Using scanning electron microscopy (SEM), the surface morphology of the nanoparticles was examined. SEM analysis shows that the Ab-AgNPs have a spherical shape. The single SPR peak also detected in the UV-Visible spectra of Ab-AgNPs indicates the development of spherical particles, which is corroborated by a SEM micrograph.

X-ray diffraction (XRD) analysis

The structure and crystalline size of the synthesized Ab-AgNPs were investigated using XRD. The XRD analysis of Ab-AgNPs revealed diffraction peaks at 34.3°, 38.6°, 45.2°, 65.9°, and 76.6°. The peaks correspond to the planes (122), (111), (200), (220), and (311) faces of silver crystal. The high peaks in the XRD study suggested an active silver composition with indexing. The average sizes of the Ab-AgNPs were found to be 52.12 nm for the facets of the face-centered cubic (fcc) crystal structure of silver nanoparticles.

Transmission electron microscopic (TEM) analysis

Transmission electron microscopy (TEM) analysis was applied to enhance the understanding of the morphology and size of the particles [30]. TEM offers superior spatial resolution in comparison to scanning electron microscopy (SEM) and allows for a more comprehensive examination of nanoparticles. TEM micrographs were recorded the synthesized Ab-AgNPs, including an HR-TEM image and a selected area electron diffraction (SAED) pattern. These images, exhibited in Figure 2a and 2b, clearly demonstrate that the Ab-AgNPs have a spherical form in the present study. The TEM observation clearly demonstrated that the silver NPs produced were predominantly spherical in shape, with sizes ranging from 1 to 40 nm and 1 to 25 nm, respectively. The present investigation established that the particles exhibited a spherical shape and varied in size, ranging from 15.24 nm to 33.45 nm. The EDS contour indicates a significant silver signal, flanked by rather quiet oxygen and carbon peaks, most likely resulting from macromolecules following to the surface of the silver nanoparticles (see Figure 3). The image also displays silver clusters of tiny particles and a few scattered nanoparticles, validating the findings acquired using SEM.

Anticancer activity of AB-AGNPS

Cell viability assays are essential for understanding the intricate cellular reactions to toxic substances. These assays help researchers evaluate the cytotoxic effects of different compounds and gain insights into the mechanisms of cellular damage. They provide information on cell survival, cell death, and the maintenance of vital metabolic processes [39]. The present study examined the effect of Ab-AgNPs on cancer cell viability. The MTT assay was used to assess the anti-cancer activity of Ab-AgNPs against MCF-7 cells. Concentrations ranging from 2.5 to 15 µg/mL have been evaluated. The results revealed that there was a reduction in cell viability that was directly proportional to the dosage. Ab-AgNPs displayed a notable toxic effect on MCF-7 cells. Silver nanoparticles in vitro reduced the viability of MCF-7 cell lines with IC_{50} values of 10 µg/ml, which indicating the potential for regulating human breast cancer. The cytomorphological variations induced by Ab-AgNPs on MCF-7 cell lines at varying concentrations (7.5, 10 µL) include intracellular activation of programmed cell death, characterized by cell shrinkage, detachment, membrane blebbing, and distorted shape. These changes are accompanied by a biochemical response that triggers apoptosis, as depicted in Figure 4. The data clearly demonstrate that the apoptosis rate of MCF-7 cell lines is directly proportional to the concentration of Ab-AgNPs. Cell inhibition shows a proportional rise based on the dosage after being exposed for 24 hours. The IC_{50} value for cell inhibition by Ab-AgNPs was determined to be 10 µg/mL. The study concluded that plant-mediated Ab-AgNPs at a dose of 10 µg/mL effectively suppressed breast cancer cell lines by 99%. These data demonstrate a correlation between the dosage and duration of exposure to an increase in cytotoxicity. The IC_{50} value indicates that the plant-mediated Ab-AgNPs have potential as an effective medication for chemotherapeutic therapy. Dipankar et al. found that moderate concentrations of AuNPs induce apoptosis in malignant cells. AuNPs are currently used in biological fields such as chemotherapy and drug delivery, following clinical laboratory testing [40].

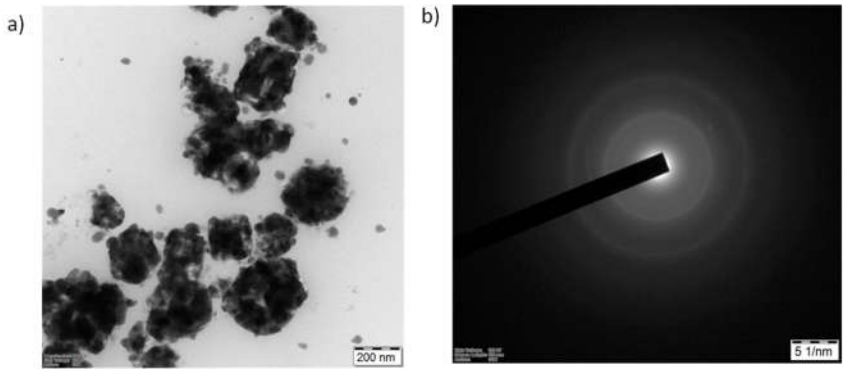

Figure 2. a) HR-TEM and b) SAED pattern of Ab-AgNPs.

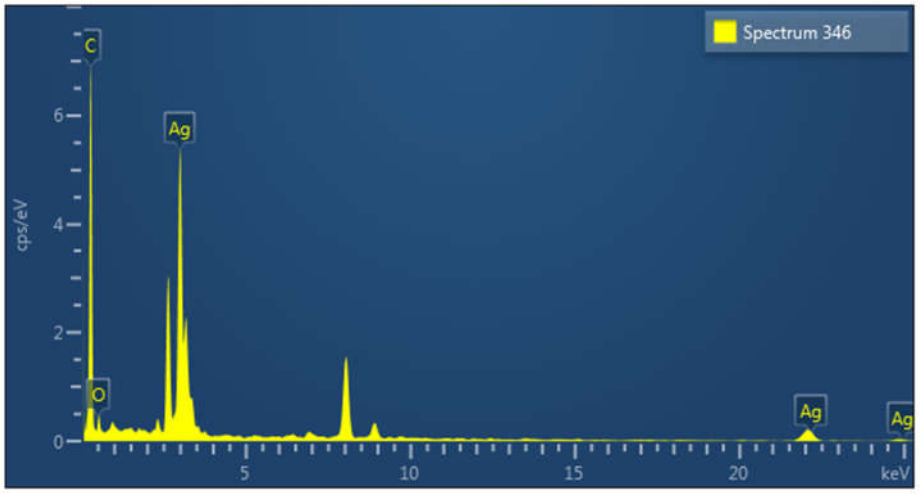

Figure 3. EDS pattern of Ab-AgNPs.

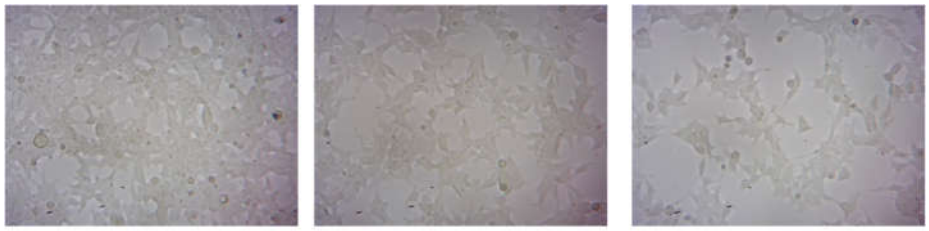

Figure 4. a) Control showed normal intact cell morphology and their images were captured by light microscope. Photomicrograph (20x) represents morphological changes in MCF-7 cells such as shrinkage, detachment, membrane blebbing and distorted shape induced by sample AgNPs treatment ((b) 7.5 and (c) 10 µg/mL for 24 h) as compared with control.

Antioxidant properties of AB-AGNPS

The antioxidant effectiveness was evaluated utilizing the DPPH technique and contrasted with the antioxidant impacts of vitamin C. The antioxidant activity of Ab-AgNPs had been determined to be 29.55%, whereas vitamin C showed an antioxidant activity of 24.28%. The results clearly show that the Ab-AgNPs demonstrate higher antioxidant efficacy compared to vitamin C. In this study, it is shown that silver nanoparticles' hydroxyl radical scavenging ability is dose dependant. The obtained findings are contrasted with the standard ascorbic acid. The study found that Ab-AgNPs had a hydrogen peroxide scavenging activity of 45.41%, whereas vitamin C had a scavenging activity of 65.63%. Green synthesised AgNPs are efficient hydroxyl radical scavengers and could be used in such circumstances. The total phenolic compounds are the main chemicals responsible for antioxidant action. The findings show that vitamin C has a significantly stronger ability to eliminate hydrogen peroxide than Ab-AgNPs.

Antimicrobial activity AB-AGNPS

The disc diffusion method has been utilized to assess the antibacterial activities of Ab-AgNPs against Gram-positive *staphylococcus aureus* and Gram-negative *pseudomonas aeruginosa* bacteria [39], as represented in Figure 5. Ab-AgNPs exhibited significant antibacterial efficacy, as indicated by the larger zone of inhibition against *staphylococcus aureus* and *pseudomonas aeruginosa*. The largest area of inhibition seen at the highest concentration of Ab-AgNPs was 26 mm and 28 mm against *staphylococcus aureus* and *pseudomonas aeruginosa*, respectively. The antibacterial activity of Ab-AgNPs was shown to be stronger against *pseudomonas aeruginosa* compared to *staphylococcus aureus*, and this difference was observed in a dose-dependent manner. The mechanism by which AgNPs operate against bacteria is not well comprehended at now. There are multiple hypotheses that explain the antibacterial action of silver nanoparticles. Firstly, it is believed that silver nanoparticles generate reactive oxygen species. Secondly, the release of Ag^{+} ions from silver nanoparticles causes proteins to denature by interacting with sulfhydryl groups.

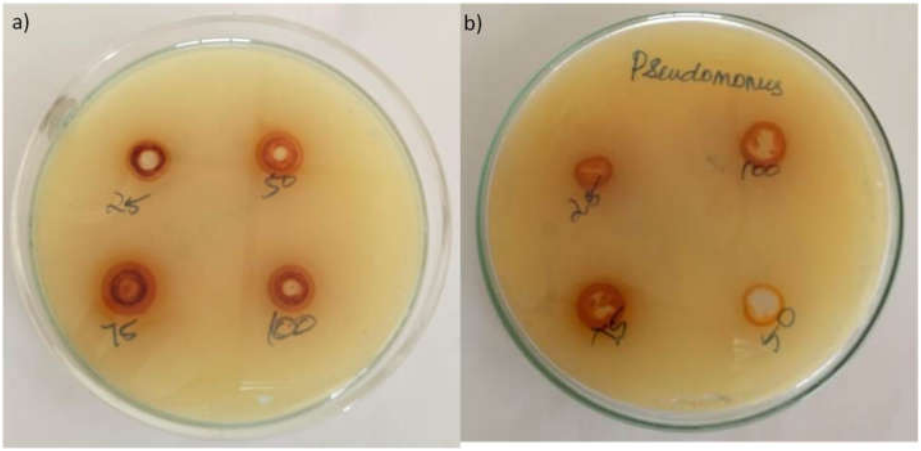

Figure 5. Antimicrobial activity of Ab-AgNPs against bacterial pathogens.

Lastly, it is thought that silver nanoparticles adhere to bacteria and cause damage to them. The limited available literature on the antibacterial effects of silver nanoparticles against gram-negative and gram-positive bacteria indicates that silver nanoparticles exhibit a modest level of antibacterial activity specifically against gram-positive bacteria. Ab-AgNPs demonstrated potent suppression against both gram positive and negative bacteria, indicating that the antibacterial efficacy of AgNPs remains unaffected by variations in the bacterial cell wall.

Molecular docking calculations

In this docking analysis, 3D structures of protein targets ERα (PDB ID: 1G50) were retrieved from the RCSB Protein Data Bank. Materials Studio and Biovia Discovery Studio 2017 software were used in this study [41]. The Aristolochic acids (AA1 and AA2) are the main phytoconstituents in the *Aristolochia bracteolate.* Since the silver nanoparticles interacted with the AA1 and AA2 using materials studio software. In this analysis, the silver nanoparticles have directly interacted with the aromatic carbon atoms of the Aristolochic acids (AA1 and AA2 Figure 6 and 7). It indicates that two molecules of *Aristolochia bracteolate* were mainly involved in the synthesis of the silver nanoparticle.

The silver-doped Aristolochic acid (AA1) was subjected to the evaluation of breast cancer activity using molecular docking analysis. In the docking analysis, the silver-doped Aristolochic acid shows a good molecular interaction energy (-25.65 kcal/mol). During the molecular interaction with $1G_{50}$, the NO_2 forms one strong hydrogen bond with the Asp 351 amino acid. The Leu 525 and Met 528 amino acids of the active site amino acid show the Pi-Alkyl interaction with the Aristolochic acid (AA1). In silver-doped Aristolochic acid (AA2) analysis, the Leu 536 forms a strong hydrogen bond with the aromatic benzene group of the Aristolochic acid (AA2). Additionally, Glu 380, Val 376, Glu 542 and Asp 538 form the non-bonded van der Waals interaction with the Aristolochic acid (AA2). The molecular docking energy of the Aristolochic acid (AA2) is -26.15 kcal/mol. In conclusion, both silver-doped Aristolochic acid (AA1 and AA2) shows good binding interaction with the active site of the $1G_{50}$ target protein.

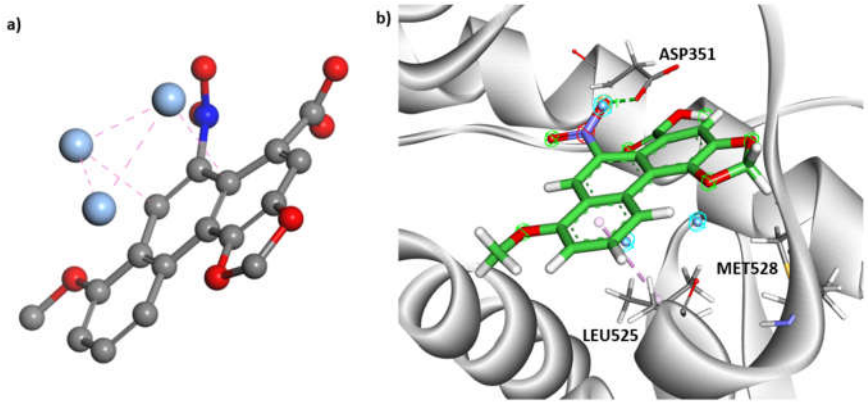

Figure 6. a) Aristolochic acid (AA1) with Silver nanoparticles interaction and b) its 3D molecular interaction with $1G_{50}$ target protein.

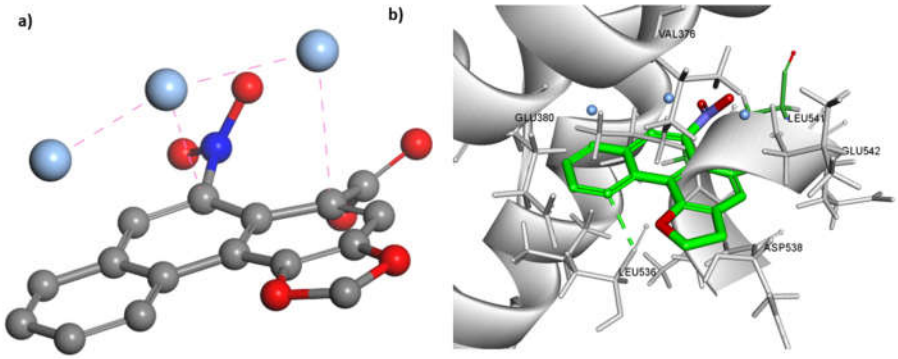

Figure 7. a) Aristolochic acid (AA2) with Silver nanoparticles interaction and b) its 3D molecular interaction with $1G_{50}$ target protein

Theoretical calculations

The molecular geometries of AA1, AA2, AA1-Ag6 and AA2-Ag6 have been studied at the B3LYP/6-311++G (d,p) level. The computed aromatic C-C and C=C, bond lengths fall on 1.38-1.40 Å and 1.36-1.37 Å. In addition C-O, C=O, C-N bond lengths fall on 1.43-1.44 Å, 1.26 Å and 1.47 Å. Furthermore computed Ag-O, Ag-Ag bond lengths arise at 2.05 Å and 2.75 Å, respectively. The theoretically calculated electronic transition peaks found at 434.56 nm, 406.12 nm, 512.84 nm, and 498.35 nm for AA1, AA2, AA1-Ag6, and AA2-Ag6 are shown in Figure S9. In order to obtain more information about the adsorption qualities, this study's analysis of global quantum molecular computations was conducted. The stability and reactivity of the systems under observation can be clearly understood from the HOMO and LUMO energies, according to Koopmans' theorem [30]. The HOMO reflects the propensity to give an electron, whereas the LUMO serves as an electron acceptor, so enabling the capacity to accept electrons [42-46]. Evidently, the band gap values decreased for all the nanocages macromolecules, underscoring a strong interaction between macromolecule and silver nanocage. The small energy gap values may suggest strong support for increased charge transfer, within the system. Figures 8 and 9 depicted FMOs AA1 and AA2. Table 1 shows that AA1 and AA2 energy gap as 3.3506 eV and 3.3704 eV, while AA1-Ag6, and AA2-Ag6 as 0.9345 eV and 1.0912 eV. We commonly assume a clear connection between the optical properties of metal clusters and their computed HOMO-LUMO energy gap in the absence of quantifiable data regarding their optical attributes. Figures 8 and 9 illustrate the silver nanocaged AA1 and AA2 molecular orbitals. The assumption is based on the relationship between the optical properties of clusters and the behavior of electrons in those systems. The chemical potential (μ) is crucial in explaining the reactivity and stability of molecules. The chemical potential, hardness, and stability of a molecule are closely correlated with its band gap, but there is an inverse relationship between band gap and chemical reactivity. The computed results unequivocally demonstrate that nanocages macromolecules exhibit higher reactivity compared to macromolecules. Hardness (η) and softness (σ) are significant characteristics that describe the behavior of a molecule during a chemical reaction. Essentially, molecules with a high level of strength have a notable challenge in changing their electronic distribution over a reaction, whereas molecules with a more flexible nature have little resistance in altering their electronic distribution throughout a reaction. Electrophilicity (ω) is a parameter that predicts the tendency of a chemical species to operate as an electrophile. It quantifies the molecule's ability to receive an electron, with higher values of ω indicating a stronger electrophilic nature. The nanocages macromolecules have been determined to possess a high electrophilicity

value, indicating their superior electrophilic nature compared to other macromolecules. It is widely known that medicines with a strong electrophilic nature possess powerful antibacterial and anticancer effects.

The molecular electrostatic potential (MEP) map is a valuable tool for investigating the reactivity of a molecule since it provides information about the locations where electrophilic and nucleophilic assaults are likely to occur based on the distribution of electron density [45-49]. The MEP image can be analyzed by employing the red-yellow-green-blue colour spectrum and various electrostatic potential levels [50-53]. The presence of blue coloration on the map signifies a region with a positive electrostatic potential, indicating a deficiency of electrons and making it vulnerable to nucleophilic attack. In the image, the green color shows areas with a neutral potential, while the red color highlights regions with a negative electrostatic potential. This suggests that these areas have an abundance of electrons, making them more susceptible to electrophilic attack. Oxygen atoms exhibited negative potential zones, whereas hydrogen atoms in AA1 and AA2 have positive potential regions. In addition, the MEP maps of the nanocage macromolecules AA1-Ag6 and AA2-Ag6 revealed that the oxygen atoms bonded to the positively charged silver atoms in the silver nanocages have a negative electrostatic potential. This makes them susceptible to electrophilic attack. On the other hand, the hydrogen atoms have regions of positive potential. The results offer understanding of the active areas where the AA1 and AA2 macromolecules interact with the nanocages in the observed complexes. These results align with the charge transfer pattern derived from the predicted dipole moments. Therefore, the findings indicate that the simulated complexes demonstrate substantial promise as possible candidates for drug delivery.

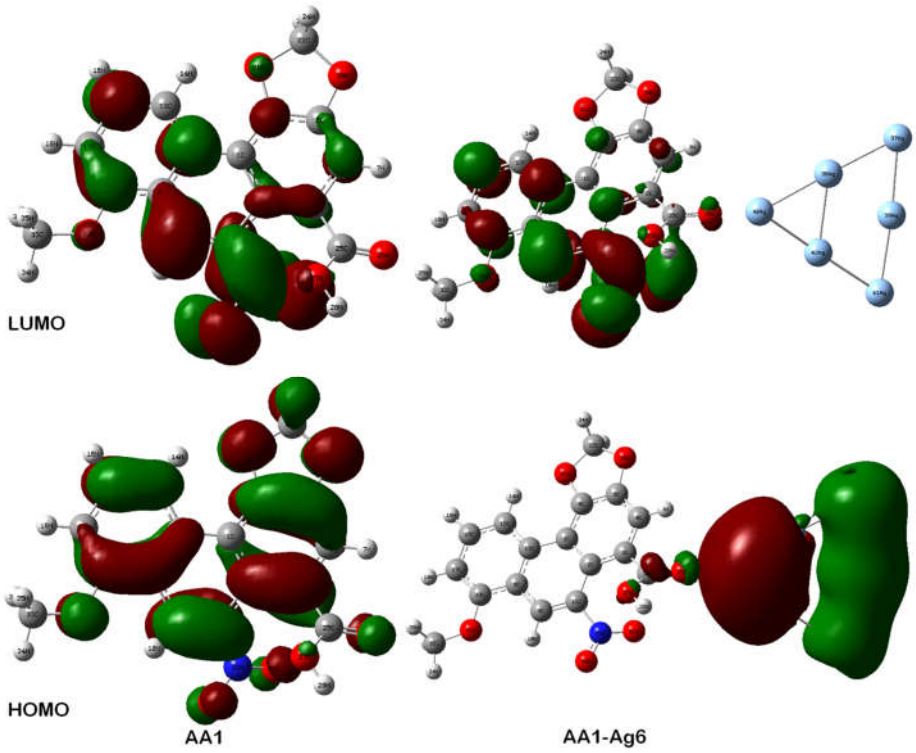

Figure 8. HOMO & LUMO plots of AA1 and AA1-Ag6.

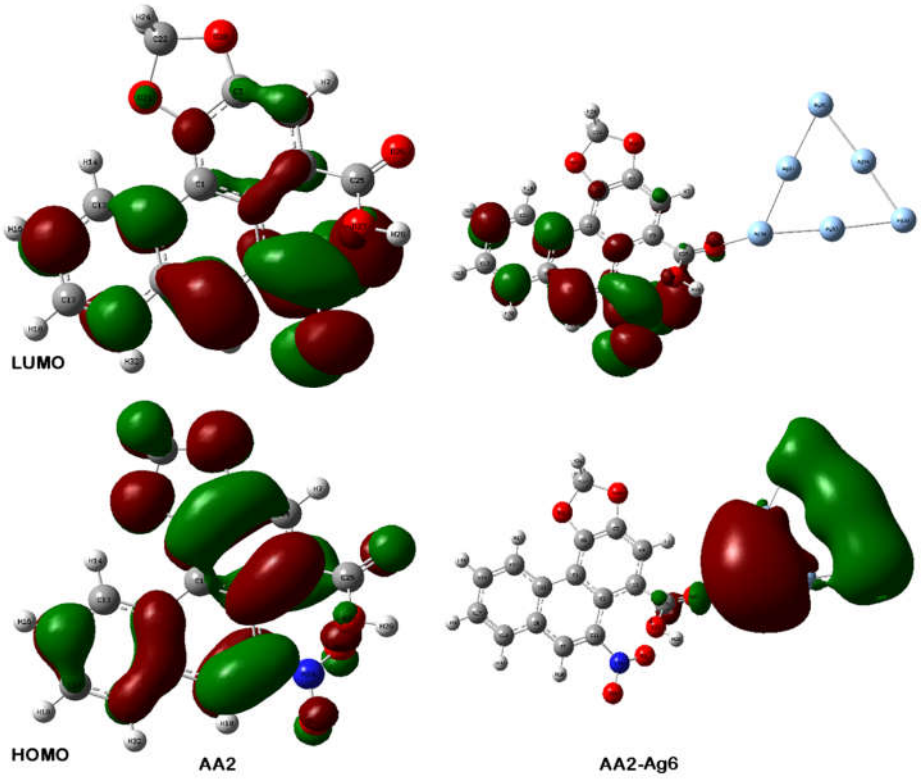

Figure 9. HOMO and LUMO plots of AA2 and AA2-Ag6.

Table 1. Physico-chemical parameters of *Aristolochia bracteolate* macro molecules and silver nano cages.

Compounds	E_{HOMO} (eV)	E_{LUMO} (eV)	IP (eV)	EA (eV)	ΔE (eV)	χ (eV)	η (eV)	σ (eV)	ω (eV)	ε (eV)	ω+ (eV)
AA1	-5.80	-2.45	5.80	2.45	3.35	-4.12	1.68	0.60	5.07	0.20	1.30
AA2	-6.00	-2.63	6.00	2.63	3.37	-4.32	1.69	0.59	5.54	0.18	1.47
AA1-Ag6	-4.43	-3.49	4.43	3.49	0.93	-3.96	0.47	2.14	16.79	0.06	8.82
AA2-Ag6	-4.69	-3.59	4.69	3.59	1.09	-4.14	0.55	1.83	15.71	0.06	7.95

CONCLUSION

The present research effectively synthesized silver nanoparticles (Ab-AgNPs) utilizing the leaf extract of the *Aristolochia bracteolate* plant through a green synthesis method. The structural properties of the synthesized Ab-AgNPs were characterized and confirmed through HR-TEM, UV-Vis, FTIR, XRD, and SEM analysis. The results showed promising cytotoxic efficacy against the MCF-7 cell line and effectiveness against both gram-positive and gram-negative bacteria. Physicochemical calculations supported the experimental data, revealing direct interaction between silver nanoparticles and aromatic carbon atoms of Aristolochic acids (AA1 and AA2).

The design suggested involvement of two *Aristolochia bracteolate* molecules in silver nanoparticle synthesis. Both experimental and theoretical studies demonstrated strong cytotoxicity activity of plant-based silver nanoparticles against cancer cell lines, indicating potential therapeutic applications.

ACKNOWLEDGMENT

This project was supported by Researchers Supporting Project number (RSPD2025R712), King Saud University, Riyadh, Saudi Arabia.

REFERENCES

1. Rajalakshmi, T.U.; Esaivani, C.; Kumar, T.A.; Mariselvam, R.; Selvan, G.T.; Zhang, Z.; Alyam, N.M.; Mariselvi, P. Green synthesis of iron oxide nanoparticles from *Spermacoce ocymoides Burm.f.* plant extracts for targeted lung cancer A549 cell therapy. *Bull. Chem. Soc. Ethiop*. **2024**, 38, 123-134.
2. Religioni, U. Cancer incidence and mortality in Poland, *Clin. Epidemiol. Glob. Health* **2020**, 8, 329-334.
3. Gatasheh, M.K. Synthesis and characterization of silver nanoparticles from *Cocos nucifera* L. male flowers: An investigation into their potent antibacterial and anticancer efficacy. *Bull. Chem. Soc. Ethiop*. **2024**, 38, 715-724.
4. Mani, M.; Okla, M.K.; Selvaraj, S.; Kumar, A.R.; Kumaresan, S.; Muthukumaran, A.; Kaviyarasu, K.; El-Tayeb, M.A.; Elbadawi, Y.B.; Almaary, K.S.; Almunqedhi, B.M.A.; Elshikh, M.S. A novel biogenic *Allium cepa* leaf mediated silver nanoparticles for antimicrobial, antioxidant, and anticancer effects on MCF-7 cell line. *Environ. Res*. **2021**, 198, 111199.
5. Ebrahimzadeh, M.A.; Hashemi, Z.; Mohammadyan, M.; Fakhar, M.; Mortazavi-Derazkola, S. In vitro cytotoxicity against human cancer cell lines (MCF-7 and AGS), antileishmanial and antibacterial activities of green synthesized silver nanoparticles using *Scrophularia striata* extract. *Surf. Interfaces* **2021**, 23, 100963.
6. Gomathi, A.C.; Rajarathinam, S.R.X.; Sadiq, A.M.; Rajeshkumar, S. Anticancer activity of silver nanoparticles synthesized using aqueous fruit shell extract of *Tamarindus indica* on MCF-7 human breast cancer cell line. *J. Drug Del. Sci. Technol*. **2020**, 55, 101376.
7. Khatun, N.; Ruhul-Amin, Md.; Parvin, S.; Siddika, A.; Hasan, I.; Kabir, S.R.; Asaduzzaman, A.K.M. Green synthesis of silver/silver chloride nanoparticles derived from *Elaeocarpus floribundus* leaf extract and study of its anticancer potential against EAC and MCF-7 cells with antioxidant and antibacterial properties. *Results Chem*. **2024**, 7, 101287.
8. Mohamed, M.S.; Idris, M.T.; Khedr, A.I.; AlGadir, H.A.; Takeshita, S.; Shah, M.M.; Ichinose, Y.; Maki, T. Activity of *Aristolochia bracteolata* against *Moraxella catarrhalis*. *Int.J.Bacteriol*. **2014**, 2014, 481686.
9. Amit,T. Medicinal use of *Aristolochia bracteolata* Lam. *J. Pharmacogn. Phytochem.* **2017**, 6, 598-599.
10. Thanh, N.C.; Pughngazhendhi, A.; Chinnathambi, A.; Alharbi, S.A.; Subramani, B.; Brindhadevi, K.; Whangchai, N.; Pikulkaew, S. Silver nanoparticles (AgNPs) fabricating potential of aqueous shoot extract of *Aristolochia bracteolata* and assessed their antioxidant efficiency. *Environ. Res*. **2022**, 208, 112683.
11. Narayanan, M.; Priya, S.; Natarajan, D.; Alahmadi, T.A.; Alharbi, S.A.; Ramakrishnan, K.; Chi. N.T.L; Pugazhendhi, A. Phyto-fabrication of silver nanoparticle using leaf extracts of *Aristolochia bracteolata* Lam and their mosquito larvicidal potential. *Process Biochem*. **2022**, 121, 163-169.
12. Ragavendran, C.; Chinnaperumal, K.; Cherian, T.; Thamilchelvan, K.; Govindasamy, B.; Vetrivel, C.; Vivekanandhan, P.; Peijnenburg, W.; Krutmuang, P. Eco-friendly

phytofabrication of silver nanoparticles using aqueous extract of *Aristolochia bracteolata* Lam: its antioxidant potential, antibacterial activities against clinical pathogens and malarial larvicidal effects. *Biomass Conv. Bioref.* **2023**. DOI: 10.1007/s13399-023-03750-8.

13. Kumaran, S.; Vetrivelan, V.; Muthu, S.; Al-Saadi, A.A. Computational analysis of anti-cancer drug hydroxyurea adsorption on nanocages of gold, silver and copper: SERS and DFT assessment. *Heliyon* **2024**, 10, e24475.
14. Venkatesh, G.; Haseena, S.; Vennila, P.; Sixto-López, Y.; Siva, V.; Mishma, J.N.C.; Azad, S.A.K.; Mary, Y.S. Solvation effects, structural, vibrational analysis, chemical reactivity, nanocages, ELF, LOL, docking and MD simulation on Sitagliptin. *Chem. Phys. Impact*. **2024**, 8, 100481.
15. Venkatesh, G.; Vennila, P.; Balasubramaniyan, S. Solvent effects, chemical reactivity, docking and antimicrobial activity of silver and gold nanocages glimepiride: Experimental and theoretical calculations. *Chem. Phys. Impact.* **2024**, 8, 20 100498.
16. Abraham, C.S.; Muthu, S.; Prasana, J.C.; Armaković, S.J.; Armaković, S.; Fathima Rizwana, B.; Ben Geoffrey, A.S. Spectroscopic profiling (FT-IR, FT-Raman, NMR and UV-Vis), autoxidation mechanism (H-BDE) and molecular docking investigation of 3-(4-chlorophenyl)-N,N-dimethyl-3-pyridin-2-ylpropan-1-amine by DFT/TD-DFT and molecular dynamics: A potential SSRI drug. *Comput. Biol. Chem*. **2018**, 77, 131-145.
17. Aslan, E.K.; Armaković, S.J., Armaković, S.; Özenver, N.; Özkul, C.; Gündüz, M.C. Biginelli dihydropyrimidines carrying azole rings: Synthesis, computational studies, and evaluation of alpha-glucosidase inhibitory and antimicrobial activities. *J. Mol. Struct*. **2024**, 1306, 137802.
18. Vikaraman, P.A.; Armaković, S.J., Armaković, S.; Celik, I.; Bhagyasree, J.B.; Dinesh Babu, K.V.; Rudrapal, M.; Divya, I.S. Pillai, R.R. Exploring the structural, photophysical and optoelectronic properties of a diaryl heptanoid curcumin derivative and identification as a SARS-CoV-2 inhibitor. *J. Mol. Struct*. **2023**, 1281, 135110.
19. Venkatesh, G.; Kamal, C.; Vennila, P.; Govindaraju, M.; Sheena Mary, Y.; Armakovic, S.; Armakovic, S.J.; Kaya, S.; Yohannan Panicker, C. Molecular dynamic simulations, ALIE surface, Fukui functions geometrical, molecular docking and vibrational spectra studies of tetra chloro *p*- and *m*-xylene. *J. Mol. Struct*. **2018**, 1171, 253-267.
20. Abdelgadir, A.A.; Ahmed, E.M.; Eltohami, M.S. Isolation, characterization and quantity determination of aristolochic acids, toxic compounds in *Aristolochia bracteolata* L. *Environ. Health Insights* **2011**, 5, 1-8.
21. Kuo, P.C.; Li, Y.C.; Wu, T.S. Chemical constituents and pharmacology of the *Aristolochia* (mădōu ling) species. *J. Tradit. Complement. Med*. **2012**, 2, 249-266.
22. Mosmann, T. Rapid colorimetric assay for cellular growth and survival: application to proliferation and cytotoxicity assays. *J. Immunol. Methods* **1983**, 65, 55-63.
23. Cetinkaya, Y.; Gocer, H., Menzek, A.; Gulcin, I. Synthesis and antioxidant properties of (3,4 dihydroxyphenyl)(2,3,4-trihydroxyphenyl) methanone and its derivatives. *Archiv. Pharmazie* **2012**, 345, 323-334.
24. Braca, A.; Sortino, C.; Politi, M. Antioxidant activity of flavonoids from *Licania licaniae* flora. *J. Ethnopharmacol.* **2002**, 79, 379-381.
25. Frisch, M.J.; Trucks, G.W.; Schlegel, H.B.; Scuseria, G.E.; Robb, M.A.; Cheeseman, J.R.; Scalmani, G.; Barone, V.; Mennucci, B.; Petersson, G.A.; Nakatsuji, H.; Caricato, M.; Li, X.; Hratchian, H.P.; Izmaylov, A.F.; Bloino, J.; Zheng, G.; Sonnenberg, J.L.; Hada, M.; Ehara, M.; Toyota, K.; Fukuda, R.; Hasegawa, J.; Ishida, M.; Nakajima, T.; Honda, Y.; Kitao, O.; Nakai, H.; Vreven, T.; Montgomery, J.A.; Jr.; Peralta, J.E.; Ogliaro, F.; Bearpark, M.; Heyd, J.J.; Brothers, E.; Kudin, K.N.; Staroverov, V.N.; Keith, T.; Kobayashi, R.; Normand, J.; Raghavachari, K.; Rendell, A.; Burant, J.C.; Iyengar, S.S.; Tomasi, J.; Cossi, M.; Rega, N.; Millam, J.M.; Klene, M.; Knox, J.E.; Cross, J.B.; Bakken, V.; Adamo, C.; Jaramillo, J.; Gomperts, R.; Stratmann, R.E.; Yazyev, O.; Austin, A.J.; Cammi, R.; Pomelli, C.; Ochterski,

J.W.; Martin, R.L.; Morokuma, K.; Zakrzewski, V.G.; Voth, G.A.; Salvador, P.; Dannenberg, J.J.; Dapprich, S.; Daniels, A.D.; Farkas, O.; Foresman, J.B.; Ortiz, J.V.; Cioslowski, J.; Fox, D.J. *Gaussian 09W*, *Revision D.01*, Gaussian, Inc.: Wallingford CT; **2013**.
26. *GaussView 6.0.16*, Gaussian Inc.: Wallingford CT; **2016**.
27. Koopmans, T.; Über die zuordnung von wellenfunktionen und eigenwerten zu den einzelnen elektronen eines atoms. *Physica* **1934**, 1, 104-113.
28. Pearson, R.G. Absolute electronegativity and hardness correlated with molecular orbital theory. *Proc. Natl. Acad. Sci*. **1986**, 83, 8440-8441.
29. Parr, R.G.; Szentpaly, L.V.; Liu, S. Electrophilicity index. *J. Am. Chem. Soc*. **1999**, 121, 1922-1924.
30. Venkatesh, G.; Serdaroğlu, G.; Üstün, E.; Haripriya, D.; Vennila, P.; Siva, V.; Haseena, S.; Sowmiya, V.; Pradhiksha A. Green synthesis, characterization, anti-cancer and antimicrobial activity of AuNPs extracted from *Euphorbia antiquorum* stem and flower: Experimental and theoretical calculations. *J. Drug Del. Sci. Tech*. **2024**, 95, 105583.
31. Venkatesh, G.; Vennila, P.; Kaya, S.; Ben Ahmed, S.; Sumathi, P.; Siva, V.; Premkumar, R.; Kamal, C. Synthesis and spectroscopic characterization of Schiff base metal complexes, biological activity, and molecular docking studies. *ACS Omega* **2024**, 9, 8123-8138.
32. Bourhia, M.; Haj Said, A.A.; Chaanoun, A.; El Gueddari, F.; Naamane, A.; Benbacer, L.; Khlil, N. Phytochemical screening and toxicological study of *Aristolochia baetica* Linn roots: Histopathological and biochemical evidence. *J. Toxicol*. **2019**, 2019, 8203832.
33. Victoria, V.; Georgii, V.; Dmitriy, U.; Khrokalo, L.; Skiba, M. Green synthesis, characterization of silver nanoparticals for biomedical application and environmental remediation. *J. Microbiol. Methods* **2022**, 193, 106384.
34. Skiba, M.; Victoria, V. Green bio-synthesis of silver nanoparticles and their catalytic activity for methyl orange degradation. *J. Chem. Technol. Metall.* **2022**, 57, 54-62.
35. Yun, B.H.; Sidorenko, V.S.; Rosenquist, T.A.; Dickman, K.G.; Grollman, A.P.; Turesky, R.J. New approaches for biomonitoring exposure to the human carcinogen aristolochic acid. *Toxicol. Res.* **2015**, 4, 763-776.
36. Venkatesh, G.; Sixto-López, Y.S.; Vennila, P.; Mary, Y.S.; Correa-Basurto, J.; Mary, Y.S.; Manikandan, A. An investigation on the molecular structure, interaction with metal clusters, anti-Covid-19 ability of 2-deoxy-D-glucose: DFT calculations, MD and docking simulations. *J. Mol. Struct*. **2022**, 1258, 132678.
37. Vennila, P.; Venkatesh, G.; Sixto-López, Y.S.; Kamal, C.; Kaya, S.; Serdaroğlu, G.; Landeros-Rivera, B.L. Synthesis, spectroscopic characterization, molecular docking studies and DFT calculation of novel Mannich base 1-((4-ethylpiperazin-1-yl)(2-hydroxyphenyl)methyl)naphthalen-2-ol. *J. Mol. Struct*. **2021**, 1246, 131164.
38. Raja, G.; Venkatesh, G.; Al-Otaibi, J.S.; Vennila, P.; Mary, Y.S.; Sixto-López, Y.; Synthesis, characterization, molecular docking and molecular dynamics simulations of benzamide derivatives as potential anti-ovarian cancer agents. *J. Mol. Struct*. **2022**, 1269, 133785.
39. Padalia, H.; Moteriya, P.; Chanda, S. Green synthesis of silver nanoparticles from marigold flower and its synergistic antimicrobial potential. *Arab. J. Chem.* **2015***,* 8, 732–741.
40. Dipankar, C.; Murugan, S. The green synthesis, characterization and evaluation of the biological activities of silver nanoparticles synthesized from *Iresine herbstii* leaf aqueous extracts. *Colloids Surf. B Biointerfaces*. **2012**, 98, 112-119.
41. Dassault Systèmes BIOVIA. Discovery Studio Modeling Environment, Release 2017. Dassault Systèmes; San Diego, CA, USA: **2017**.
42. Vennila, P.; Al-Otaibi, J.S.; Venkatesh, G.; Mary, Y.S.; Raj, V.; Acharjee, N.; Tamilselvi, P. Structural, spectral, molecular docking, and molecular dynamics simulations of phenylthiophene-2-carboxylate compounds as potential anticancer agents. *Polycyclic Aromat. Comp*. **2024**, 44, 238-260.

43. Venkatesh, G.; Haseena, S.; Al-Otaibi, J.S.; Mary, Y.S.; Vennila, P.; Mary, Y.S.; Azad, S.A. Observations into the reactivity, docking, DFT, and MD simulations of fludarabine and clofarabine in various solvents. *J. Mol. Liq*. **2023**, 383, 122076.
44. Elangovan, N.; Ganesan, T.S.; Vishveshwaran, A.; Arumugam, N.; Almansour, A.I.; Chandrasekar, S.; Thomas, R. Synthesis, computational, reactivity analysis, non-covalent interaction and docking studies on (N1E,N2E)-N1,N2 bis(2,4-dichlorobenzylidene)-4-methylbenzene-1,2-diamine. *J. Mol. Struct.* **2024**, 1318, 139346.
45. Aneesh, K.R.; Al-Otaibi, J.S.; Mary, Y.S.; Thomas, R.; Pillai, R.R. Solvent effects and Raman enhancement during the adsorption of atrazine on pristine Ag, Au, Cu and mixed clusters. *Comput. Theor. Chem*. **2024**, 1237, 114628.
46. Aazam, E.S.; Thomas, R. Understanding the behavior of a potential anticancer lamotrigine in explicit solvent (water and DMSO) using quantum mechanical tools and abinitio molecular dynamics. *Chem. Phys. Impact* **2024**, 8, 100404.
47. Sattar, F.; Wang, Z.; Zhou, X.; Ullah, Z. Battling hazardous gas molecules with kekulene surfaces: A computational study. *J. Mol. Liq*. **2024**, 407, 125099.
48. Ullah, Z.; Subramanian, S.; Lim, H.; Dogan, N.A.; Lee, J.S.; Nguyen, T.S.; Yavuz, C.T. Highly selective and scalable molecular fluoride sensor for naked-eye detection. *ACS Appl. Mater. Interfaces* **2024**, https://doi.org/10.1021/acsami.4c01187.
49. Ullah, Z.; Kim, K.; Venkanna, A.; Kim, H.S.; Kim, M.I.; Kim, M-H. Plausible pnicogen bonding of epi-cinchonidine as a chiral scaffold in catalysis. *Front. Chem.* **2021**, 9, 669515.